Spatial, spectral and temporal coherence of ultra-intense twin beams

Jan Peřina Jr.*
RCPTM, Joint Laboratory of Optics of Palacký University and Institute of Physics of Academy of Sciences of the Czech Republic, Faculty of Science, Palacký University, 17. listopadu 12, 77146 Olomouc, Czech Republic

Using the model of parametric interaction based on the spatio-spectral Schmidt modes and generalized parametric approximation, we analyze coherence and mode structure of ultra-intense twin beams generated in the regime with pump depletion. We show that the increase of spatial and spectral coherence with the increasing pump power observed for moderate powers is replaced by the decrease for the pump powers at which pump depletion occurs. This behavior of coherence is opposed to that exhibited by the number of spatio-spectral modes effectively constituting the twin beam. The conditions for maximal coherence are analyzed considering pump-beam parameters (spectral width, transverse radius). The existence of additional coherence maxima occurring at even higher pump powers is predicted and explained by the oscillatory evolution of the modes' populations.

PACS numbers: 42.65.Lm,42.65.Yj,42.50.Dv

I. INTRODUCTION

Parametric down-conversion (PDC) has been used the most frequently in its 'weak' spontaneous regime where it provides entangled photon pairs with genuine quantum properties. On the other hand, it provides the so-called twin beams containing a large number of photon pairs when intensively pumped. Such twin beams exhibit ideally perfect correlations in the photon numbers (or intensities) of the signal and idler fields that constitute the twin beam [1–4]. These correlations in photon numbers occur in the spectrum as well as in the fields' transverse planes as a consequence of energy conservation and phase-matching conditions, respectively. However, as pulsed pumping is needed to generate intense twin beams and the nonlinear interaction is restricted to a final volume of the nonlinear material, neither spectral nor spatial correlations inside the twin beam are ideal. For this reason, we introduce spectral and spatial intensity correlation functions to characterize properties of the real twin beams.

The spectral and spatial intensity correlation functions of twin beams have been experimentally analyzed in three regions differing by intensity. In each of them, different behavior has been observed. It has been shown that the coherence of individual photon pairs generated in the spontaneous regime is preserved even for relatively intense twin beams [5, 6]. In this first region, the pump field is sufficiently intense relative to the overall strength of the nonlinear interaction (including the interaction length) so that no pump depletion occurs. The twin beam is thus composed of a large number of weakly populated signal and idler modes.

An increase in the spatial and spectral coherence of a twin beam is characteristic for the second region [7–12]. The theory and its comparison with the experimentally determined numbers of twin-beam modes have revealed that greater mean photon numbers in individual signal and idler Schmidt modes occur in this region [13]. Moreover, the mean photon numbers of the most intense signal and idler modes are such that the pump depletion has to occur during the interaction. The increase of coherence observed in this region has been explained by the dominance of the Schmidt modes with the greatest Schmidt coefficients over the other Schmidt modes. The reason is that the number of highly-populated modes is smaller and so the twin beam exhibits better coherence properties. Decrease in the number of modes accompanying the increase of coherence has been experimentally confirmed in [14].

Finally, the third region reached with ultra-intense pump beams has been investigated experimentally only recently [14–16]. Here, the coherence of the twin beam decreases whereas the number of modes increases. As shown in this paper, this behavior can be explained, similarly as in the second region, by considering the evolution of mean photon numbers of the individual signal and idler Schmidt modes. However, in this region the signal and idler Schmidt modes with the greatest Schmidt coefficients already loose their energy during the propagation, in favor of the pump modes that originally provided their energy at the beginning of the nonlinear interaction.

The three intensity regions are easily identified when the twin-beam intensity is considered as a function of pump power. An initial exponential increase of the twin-beam intensity occurs in the first region. The area where the exponential increase is gradually replaced by the linear one forms the second region. Finally, the pump powers at which a nearly linear increase of twin-beam intensity is found belong to the third region. The values of pump powers at which such behavior is observed depend strongly on the properties of nonlinear medium. It holds in general that the smaller is the number of spatio-spectral modes, the smaller are the pump powers. Also,

*Electronic address: jan.perina.jr@upol.cz

the stronger is the nonlinear interaction, the smaller are the pump powers. From this point of view, the pump powers lower by several orders in magnitude are expected in nonlinear photonic structures (e.g., waveguides) compared to bulk crystals analyzed in this paper.

Here, we develop the theory explaining the behavior of intense twin beams in the third intensity region, i.e. when the pump depletion is substantial for twin-beam properties. We introduce *the generalized parametric approximation* in which the pump beam is depleted during its propagation in accordance with the classical solution of the nonlinear interaction. We decompose the twin beam together with the pump beam into multiple triplets of individual spatio-spectral modes defined in the signal, idler and pump beams. We adopt the signal and idler spatio-spectral Schmidt modes defined for weak twin beams [17–20] following the approach elaborated in [13]. The presented theory represents a generalization of the theory given in [13] that assumes un-depleted pump beams. As such, it also covers the first and the second intensity regions.

The behavior of twin beams in the region with pump depletion has been successfully described replacing the initial vacuum quantum state of a twin beam by a classical statistical ensemble and then finding the nonlinear evolution numerically [14, 21]. The loss of coherence for high pump powers as well as spectral and spatial deformations of the pump beam have been revealed in this approach. On the other hand, the relation between the coherence and the twin-beam internal structure cannot be analyzed in this approach. For this reason, we generalize the model of Ref. [13] based on the Schmidt modes to the region with pump depletion. This allows us, among others, to predict additional coherence maxima found at high pump powers.

We note that a theory of intense twin beams based upon the quasi-monochromatic and quasi-plane-wave pump-field approximations has been developed for the pump powers belonging to the second region [22–25]. Similarly as the presented theory, this theory has been based on the solution of the linear Heisenberg equations. The suggested generalized parametric approximation could be applied also here with the potential to generalize the existing theory into the region with pump depletion.

The developed theory is suitable not only for parametric interactions [26]. It can be applied also to nonlinear resonant interactions involving four-wave mixing in cold atomic ensembles [27–29] in which high effective nonlinear coupling constants occur.

The paper is organized as follows. In Sec. II, the theory of intense twin beams in the pump-depleted regime is developed and quantities characterizing twin beams are defined. Spatial, spectral and temporal coherence of twin beams is discussed in Sec. III. Multiple coherence maxima observed with the increasing pump power and their relation to the twin-beam structure are analyzed in Sec. IV. A model with an extended interaction length is briefly discussed in Sec. V. Conclusions are drawn in Sec. VI.

II. THE MODEL OF ULTRA-INTENSE TWIN BEAMS INVOLVING PUMP DEPLETION

An intense twin beam is generated in the process of PDC in which the pump field interacts nonlinearly with the signal and idler fields. The signal and idler fields are assumed initially in the vacuum states. They take energy from the pump field during the interaction. The nonlinear interaction mediated by the material with $\chi^{(2)}$ nonlinearity is described by the following nonlinear interaction momentum operator $\hat{G}_{\rm int}$ [26, 30, 31]:

$$\hat{G}_{\rm int}(z) \;=\; 2\epsilon_0 \int dxdy \int dt \left[\chi^{(2)} \hat{E}_{\rm p}^{(+)}(\mathbf{r},t)\hat{E}_{\rm s}^{(-)}(\mathbf{r},t)\hat{E}_{\rm i}^{(-)}(\mathbf{r},t) + {\rm h.c.}\right]; \quad (1)$$

$\mathbf{r} = (x,y,z)$. In Eq. (1), $\hat{E}_{\rm p}^{(+)}$ denotes the positive-frequency pump electric-field operator amplitude whereas $\hat{E}_{\rm s}^{(-)}$ [$\hat{E}_{\rm i}^{(-)}$] stands for the negative-frequency part of the signal [idler] electric-field operator amplitude. The vacuum permittivity is denoted as ϵ_0 and h.c. replaces the Hermitian conjugated term. The electric-field amplitudes $\hat{E}_a$, $a = {\rm p,s,i}$, are assumed to be decomposed into the basis of monochromatic plane waves that have their photon annihilation and creation operators.

To reveal a spatio-spectral structure of the fields suitable for describing the nonlinear interaction we first consider the generation of individual photon pairs in the weak nonlinear interaction. In this case, the pump field is treated classically and an emitted photon pair is described by a quantum state $|\psi\rangle_{\rm si}$ obtained by the first-order perturbation solution of the corresponding Schrödinger equation. This solution allows us to find suitable spatio-spectral Schmidt dual modes (identified by triple indices mlq) and then to associate with them the signal- and idler-field creation operators $\hat{a}^\dagger_{{\rm s},mlq}$ and $\hat{a}^\dagger_{{\rm i},mlq}$, respectively. Assuming for simplicity the factorization of modes into their spatial (indices ml) and spectral (q) parts, the state $|\psi\rangle_{\rm si}$ is written as (for more details, see [13]):

$$|\psi\rangle_{\rm si} = t^\perp f^\parallel \sum_{m,l,q} \lambda^\perp_{ml}\lambda^\parallel_q \hat{a}^\dagger_{{\rm s},mlq}\hat{a}^\dagger_{{\rm i},mlq}|{\rm vac}\rangle; \quad (2)$$

$|{\rm vac}\rangle$ stands for the signal- and idler-field vacuum state. The coefficients $\lambda^\perp_{ml}$ ($\lambda^\parallel_q$) give the probability amplitudes of having an ml-th (q-th) spatial (spectral) mode in the generated state. Symbol $t^\perp$ ($f^\parallel$) denotes an appropriate spatial (spectral) normalization constant. The Schmidt-mode creation operators $\hat{a}^\dagger_{b,mlq}$ occurring in Eq. (2) are given as linear combinations of the monochromatic (frequency ω_b) plane-wave (radial transverse wave-

vector coordinates $k_b^{\perp}$ and φ_b) mode creation operators $\hat{a}_b^{\dagger}(k_b^{\perp},\varphi_b,\omega_b)$:

$$\hat{a}_{b,mlq}^{\dagger} = \int_0^{\infty} dk_b^{\perp} \int_0^{2\pi} d\varphi_b \int_0^{\infty} d\omega_b\, t_{b,ml}(k_b^{\perp},\varphi_b) \times f_{b,q}(\omega_b)\hat{a}_b^{\dagger}(k_b^{\perp},\varphi_b,\omega_b), \qquad b=\mathrm{s,i}. \quad (3)$$

In Eq. (3), the Schmidt mode functions $t_{b,ml}$ and $f_{b,q}$ defined in the beam's transverse wave-vector plane [32, 33] and the frequency domain [34], respectively, have been used.

Modes in the pump field can be assigned to individual pairs of the signal and idler Schmidt modes obtained at the single photon-pair level. This results in mutually independent modes' triplets. They can be conveniently used for rewriting the momentum operator $\hat{G}_{\mathrm{int}}$ in the approximative form:

$$\hat{G}_{\mathrm{int}}^{\mathrm{av}}(z) = -i\hbar K \sum_{m=-\infty}^{\infty}\sum_{l,q=0}^{\infty} \hat{a}_{\mathrm{p},mlq}(z)\hat{a}_{\mathrm{s},mlq}^{\dagger}(z)\hat{a}_{\mathrm{i},mlq}^{\dagger}(z) + \mathrm{h.c.}; \quad (4)$$

$\hbar$ stands for the reduced Planck constant. A common coupling constant K introduced in Eq. (4) includes multiplicative factors $t^{\perp}f^{\parallel}$ quantifying the strength of nonlinear interaction in the medium of length L and normalization with respect to photon numbers (ξ_{p}); $K = t^{\perp}f^{\parallel}/(L\xi_{\mathrm{p}})$. The pump power P_{p}, its repetition rate f and its central frequency ω_{p}^0 determine the overall pump-field amplitude ξ_{p} in the form $\xi_{\mathrm{p}} = \sqrt{P_{\mathrm{p}}/(f\hbar\omega_{\mathrm{p}}^0)}$. It is assumed that the pump power P_{p} can be divided into individual pump modes indexed by mlq linearly proportionally to their squared Schmidt coefficients $(\lambda_{ml}^{\perp}\lambda_q^{\parallel})^2$. This means that an initial classical (coherent) amplitude $A_{\mathrm{p},mlq}^{\mathcal{N}}(0) = \lambda_{ml}^{\perp}\lambda_q^{\parallel}\xi_{\mathrm{p}}$ is assigned to an (mlq)-th mode.

The Heisenberg equations derived from the momentum operator $\hat{G}_{\mathrm{int}}^{\mathrm{av}}$ in Eq. (4) are written for individual modes' triplets as follows:

$$\begin{aligned}
\frac{d\hat{a}_{\mathrm{s},mlq}(z)}{dz} &= K\hat{a}_{\mathrm{p},mlq}(z)\hat{a}_{\mathrm{i},mlq}^{\dagger}(z),\\
\frac{d\hat{a}_{\mathrm{i},mlq}(z)}{dz} &= K\hat{a}_{\mathrm{p},mlq}(z)\hat{a}_{\mathrm{s},mlq}^{\dagger}(z),\\
\frac{d\hat{a}_{\mathrm{p},mlq}(z)}{dz} &= -K\hat{a}_{\mathrm{s},mlq}(z)\hat{a}_{\mathrm{i},mlq}(z). \quad (5)
\end{aligned}$$

The operator equations (5) are nonlinear. They can be solved exactly only for the interacting fields with small photon numbers invoking numerical approach. Here, we find an approximative solution using the fact that the pump field remains strong during the interaction. We treat it classically and express its evolution along the nonlinear medium using the solution of classical nonlinear equations. We further pay attention to one typical modes' triplet and omit the indices mlq for simplicity. We transform the Heisenberg operator equations (5) into their classical analog written for fields' amplitudes determined for the symmetric ordering of fields' operators:

$$\begin{aligned}
\frac{dA_{\mathrm{s}}(z)}{dz} &= KA_{\mathrm{p}}(z)A_{\mathrm{i}}(z),\\
\frac{dA_{\mathrm{i}}(z)}{dz} &= KA_{\mathrm{p}}(z)A_{\mathrm{s}}(z),\\
\frac{dA_{\mathrm{p}}(z)}{dz} &= -KA_{\mathrm{s}}(z)A_{\mathrm{i}}(z). \quad (6)
\end{aligned}$$

In the symmetric ordering, $A_{\mathrm{p}}(0) = \sqrt{(A_{\mathrm{p}}^{\mathcal{N}})^2(0)+1/2}$ and $A_{\mathrm{s}}(0) = A_{\mathrm{i}}(0) = 1/\sqrt{2}$ for the initial vacuum signal- and idler-field amplitudes.

As the signal and idler fields occur symmetrically in PDC and they both begin the interaction in the vacuum state, their classical amplitudes are equal, i.e. $A_{\mathrm{s}}(z) = A_{\mathrm{i}}(z)$. This together with the integral of motion $A_{\mathrm{p}}^2(z) + A_{\mathrm{s}}^2(z) = A_{\mathrm{p}}^2(0) + A_{\mathrm{s}}^2(0) \equiv A_{\mathrm{ps}}^2$ and assumption of real amplitudes A_{p}, A_{s} and A_{i} and real coupling constant K allows to solve Eqs. (6) analytically. In detail, the third equation in (6) is transformed into a differential equation for $A_{\mathrm{p}}(z)$ that can be solved by direct integration. The integral of motion then provides the signal- and idler-field amplitudes $A_{\mathrm{s}}(z)$ and $A_{\mathrm{i}}(z)$:

$$A_{\mathrm{p}}(z) = A_{\mathrm{ps}}\frac{A_{\mathrm{p}}\cosh(KA_{\mathrm{ps}}z) - A_{\mathrm{ps}}\sinh(KA_{\mathrm{ps}}z)}{A_{\mathrm{ps}}\cosh(KA_{\mathrm{ps}}z) - A_{\mathrm{p}}\sinh(KA_{\mathrm{ps}}z)}, \quad (7)$$

$$A_{\mathrm{s}}(z) = \frac{A_{\mathrm{s}}A_{\mathrm{ps}}}{A_{\mathrm{ps}}\cosh(KA_{\mathrm{ps}}z) - A_{\mathrm{p}}\sinh(KA_{\mathrm{ps}}z)}; \quad (8)$$

$A_{\mathrm{p}} \equiv A_{\mathrm{p}}(0)$ and $A_{\mathrm{s}} \equiv A_{\mathrm{s}}(0)$. The solution written in Eqs. (7) and (8) has been obtained for the nonzero pump field $A_{\mathrm{p}}(z)$. The pump field is completely depleted at $z = z_0$ for which $A_{\mathrm{p}}(z_0) = A_{\mathrm{s}} = 1/\sqrt{2}$:

$$z_0 = \frac{1}{2KA_{\mathrm{ps}}}\ln\left[1 + \frac{2A_{\mathrm{ps}}}{A_{\mathrm{ps}}+A_{\mathrm{s}}}\frac{A_{\mathrm{p}}-A_{\mathrm{s}}}{A_{\mathrm{ps}}-A_{\mathrm{p}}}\right]. \quad (9)$$

At this point, the phases of the interacting fields change such that the pump field begins to take its energy back from the signal and idler fields. At the point $z = 2z_0$ all energy is back in the pump field and the evolution repeats. In the interval $z_0 \le z \le 2z_0$, the fields' evolution is again described by Eqs. (7) and (8) with the variable z substituted by $2z_0 - z$.

After finding the classical solution we return back to the operator equations (5). We assume the pump field in the classical form described in Eq. (7). This generalizes the usual parametric approximation in which the pump field is treated as a constant. We call this approach as *the generalized parametric approximation*. The Heisenberg equations for the signal- and idler-field annihilation operators then form a linear system of operator equations:

$$\begin{aligned}
\frac{d\hat{a}_{\mathrm{s}}(z)}{dz} &= KA_{\mathrm{p}}(z)\hat{a}_{\mathrm{i}}^{\dagger}(z),\\
\frac{d\hat{a}_{\mathrm{i}}(z)}{dz} &= KA_{\mathrm{p}}(z)\hat{a}_{\mathrm{s}}^{\dagger}(z). \quad (10)
\end{aligned}$$

The solution of Eqs. (10) can be found for an arbitrary pump-field profile $A_{\rm p}(z)$ in the form generalizing that found in the parametric approximation:

$$\begin{aligned}\hat{a}_{\rm s}(z) &= U(z)\hat{a}_{\rm s}(0) + V(z)\hat{a}_{\rm i}^{\dagger}(0),\\ \hat{a}_{\rm i}(z) &= U(z)\hat{a}_{\rm i}(0) + V(z)\hat{a}_{\rm s}^{\dagger}(0)\end{aligned} \tag{11}$$

and

$$U(z) = \cosh[\varphi(z)], \quad V(z) = \sinh[\varphi(z)]; \tag{12}$$

$\varphi(z) = \int_0^z dz' K A_{\rm p}(z')$. We have for the pump-field amplitude $A_{\rm p}(z)$ given in Eq. (7):

$$\varphi(z) = KA_{\rm ps}z - \ln\left[\frac{A_{\rm ps}+A_{\rm p}}{2A_{\rm ps}} + \frac{A_{\rm ps}-A_{\rm p}}{2A_{\rm ps}}\exp(2KA_{\rm ps}z)\right]. \tag{13}$$

We note that $\varphi(z) = KA_{\rm ps}z$ in the usual parametric approximation. We also note that, similarly as the parametric approximation, the generalized parametric approximation does not conserve the energy during the nonlinear interaction. In fact the energy in the signal (and idler) field given by the solution (11) is lower than that derived classically from Eq. (8). However, it can be shown that the intensity auto- and cross-correlation functions as well as numbers of modes are practically unaffected by this drawback.

The solution (11) allows us to determine physical quantities characterizing twin beams. Here, as an example, we define suitable quantities in the frequency domain. The definitions of temporal quantities as well as quantities in the transverse wave-vector plane are analogous. They can be found in [13].

The signal-field intensity spectrum $n_{{\rm s},\omega}$ averaged over the transverse modes is defined as follows:

$$\begin{aligned}n_{{\rm s},\omega}(\omega_{\rm s}) &= \langle \hat{a}_{\rm s}^{\dagger}(\omega_{\rm s},L)\hat{a}_{\rm s}(\omega_{\rm s},L)\rangle_{\perp}\\ &= \sum_{ml}\sum_{q}|f_{{\rm s},q}(\omega_{\rm s})|^2 V_{mlq}^2.\end{aligned} \tag{14}$$

Symbol $\langle\rangle_{\perp}$ stands for quantum mechanical averaging combined with averaging in the transverse wave-vector plane. The number $N_{\rm s}$ of generated signal photons is easily obtained by the formula

$$N_{\rm s} = \int_0^{\infty} d\omega_{\rm s}\, n_{{\rm s},\omega}(\omega_{\rm s}) = \sum_{ml}\sum_{q} V_{mlq}^2. \tag{15}$$

The averaged signal-field spectral intensity correlations are described by the fourth-order correlation function $A_{{\rm s},\omega}$ defined as:

$$\begin{aligned}A_{{\rm s},\omega}(\omega_{\rm s},\omega_{\rm s}') &= \langle \mathcal{N} : \Delta[\hat{a}_{\rm s}^{\dagger}(\omega_{\rm s},L)\hat{a}_{\rm s}(\omega_{\rm s},L)]\\ &\quad\times \Delta[\hat{a}_{\rm s}^{\dagger}(\omega_{\rm s}',L)\hat{a}_{\rm s}(\omega_{\rm s}',L)] :\rangle_{\perp}\\ &= \sum_{ml}\left|\sum_{q} f_{{\rm s},q}^{*}(\omega_{\rm s}) f_{{\rm s},q}(\omega_{\rm s}') V_{mlq}^2\right|^2;\end{aligned} \tag{16}$$

symbol $\mathcal{N}$ :: means the normal ordering of fields' operators.

Similarly, the spectral intensity cross-correlations between the signal and idler fields are described using the following fourth-order correlation function:

$$\begin{aligned}C_{\omega}(\omega_{\rm s},\omega_{\rm i}) &= \langle \mathcal{N} : \Delta[\hat{a}_{\rm s}^{\dagger}(\omega_{\rm s},L)\hat{a}_{\rm s}(\omega_{\rm s},L)]\\ &\quad\times \Delta[\hat{a}_{\rm i}^{\dagger}(\omega_{\rm i},L)\hat{a}_{\rm i}(\omega_{\rm i},L)] :\rangle_{\perp}\\ &= \sum_{ml}\left|\sum_{q} f_{{\rm s},q}(\omega_{\rm s}) f_{{\rm i},q}(\omega_{\rm i}) U_{mlq} V_{mlq}\right|^2.\end{aligned} \tag{17}$$

We determine entanglement dimensionality K of the twin beam [35, 36] according to the formula

$$\begin{aligned}K &= \frac{\left(\sum_{mlq}\langle \hat{a}_{{\rm s},mlg}(L)\hat{a}_{{\rm i},mlg}(L)\rangle^2\right)^2}{\sum_{mlq}\langle \hat{a}_{{\rm s},mlg}(L)\hat{a}_{{\rm i},mlg}(L)\rangle^4}\\ &= \frac{\left(\sum_{mlq} U_{mlq}^2 V_{mlq}^2\right)^2}{\sum_{mlq} U_{mlq}^4 V_{mlq}^4}\end{aligned} \tag{18}$$

that arises after defining suitable photon-pair creation and annihilation operators [37]. It quantifies the number of paired modes found in a twin beam. We note that formula (18) reduces to the usual Schmidt number [19] for weak twin beams. We also note that several quantifiers of entanglement dimensionality have been compared in [13, 38, 39].

The number of paired modes effectively present in any physical variable of the twin beam can be estimated by the corresponding Fedorov ratio K^{Δ} [40]. It is defined as the ratio of the width $\Delta n_{\rm s}$ of the signal-field intensity profile and the width $\Delta C_{\rm s}$ of the corresponding intensity cross-correlation function in a given variable, i.e.

$$K^{\Delta} = \frac{\Delta n_{\rm s}}{\Delta C_{\rm s}}. \tag{19}$$

In the following discussion, we consider a pump field with Gaussian spectrum and Gaussian transverse profile. Its positive-frequency electric-field amplitude $E_{\rm p}^{(+)}(x,y,0,t)$ in front of the crystal is expressed as follows:

$$\begin{aligned}E_{\rm p}^{(+)}(x,y,0,t) &= \sqrt{\frac{P_{\rm p}}{\epsilon_0 cf}}\sqrt{\frac{2}{\pi}}\frac{1}{w_{\rm p}}\exp\left[-\frac{x^2+y^2}{w_{\rm p}^2}\right]\\ &\quad\times\sqrt{\sqrt{\frac{2}{\pi}}\frac{1}{\tau_{\rm p}}}\exp\left[-\frac{(1+ia_p)t^2}{\tau_{\rm p}^2}\right]\exp(-i\omega_p^0 t).\end{aligned} \tag{20}$$

In Eq. (20), w_p gives the pump-beam radius, $\tau_{\rm p}$ stands for the pump-pulse duration and $a_{\rm p}$ is the pump-pulse chirp parameter. Symbol c denotes the speed of light in vacuum.

III. SPATIAL, SPECTRAL AND TEMPORAL COHERENCE OF TWIN BEAMS

To demonstrate the behavior of twin beams when the pump power P_p varies, we consider two BBO crystals 4-mm and 8-mm long both cut for non-collinear type-I process (eoo) for the spectrally-degenerate interaction pumped by the pulses at wavelength $\lambda_\mathrm{p} = 349$ nm generated with the repetition rate $f = 400$ s^{-1}. These pulses are experimentally produced by the third harmonics of the Nd:YLF laser operating at the wavelength 1.047 μm. Assuming the pump field at normal incidence, the signal and idler fields at the central wavelengths $\lambda_\mathrm{s}^0 = \lambda_\mathrm{i}^0 = 698$ nm ($\vartheta_\mathrm{BBO} = 36.3$ deg) propagate outside the crystal under the radial emission angles $\vartheta_\mathrm{s}^0 = \vartheta_\mathrm{i}^0 = 8.45$ deg. The spectral and transverse wave-vector Schmidt modes have been determined in [20] and applied for the analysis of twin beams assuming undepleted pump beams in [13]. The analyzed configuration is symmetric for the signal and idler fields. That is why we further pay attention to only the signal-field properties, together with the joint signal-idler fields' properties. In this section, we first analyze the evolution of photon-pair numbers and effective numbers of twin-beam modes (Subsec. A). Then, we study spectral (Subsec. B), spatial (Subsec. C) and temporal (Subsec. D) coherence of the twin beams.

A. Photon-pair numbers, numbers of modes

The number N_s of emitted photon pairs naturally increases with the increasing pump power P_p. Whereas the increase is exponential for smaller values of power P_p, this increase is gradually replaced by the linear one for greater powers P_p (see Fig. 1). This change originates in the fact that the mean photon numbers of the down-converted modes with the greatest Schmidt coefficients λ, that have the initial fastest growth and thus form the initial exponential growth, become saturated and even loose their energy, due to pump depletion. The initial fast exponential growth leads to the dominance of the modes with the greatest Schmidt coefficients λ over the other modes. This reduces the number K of twin-beam modes (see Fig. 2). When this dominance is lost at greater pump powers P_p due to pump depletion, the number K of modes begins to increase for the powers P_p greater than a certain threshold power $P_\mathrm{p,th}$. At this power, the down-converted modes with the greatest Schmidt coefficients λ begin to send their energy back to the corresponding pump modes whereas the modes with smaller Schmidt coefficients λ still take energy from their pump modes. This assures the continuation of the increase of the overall energy in the down-converted fields.

For a given crystal, the smaller the number K of modes (depending on pump-beam parameters), the faster the increase of the number N_s of emitted photon pairs with the power P_p. This originates from the fact that when dividing the overall power P_p into individual pump modes the pump powers of the individual modes are greater for smaller numbers K of modes. As a consequence the nonlinear interaction inside a smaller number of individual triplets is effectively more developed. This is documented in Fig. 1 for the twin beams generated by pump pulses with different spectral widths $\Delta\lambda_\mathrm{p}$. The analysis presented in [20] shows that, for the considered spectral widths, the wider the spectral width $\Delta\lambda_\mathrm{p}$, the greater the number K of modes and so the slower the increase of the number N_s of emitted photon pairs. The comparison of curves plotted in Fig. 1 for the 4-mm and 8-mm long crystals reveals that the numbers N_s of emitted photon pairs obtained in the longer crystal are smaller than those reached in the shorter crystal. This is given by the fact that individual mode triplets interact longer in the

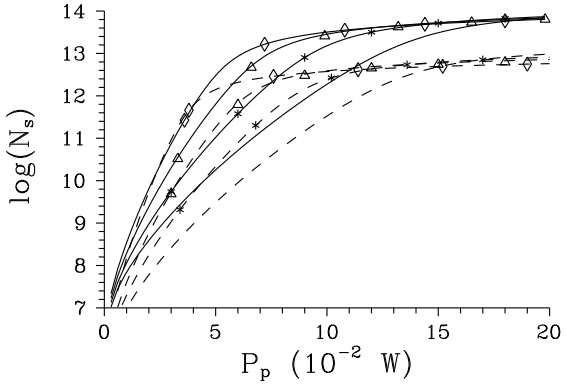

FIG. 1: Mean numbers N_s of signal photons emitted from 4-mm (solid curves) and 8-mm (dashed curves) long crystals as functions of pump power P_p for $\Delta\lambda_\mathrm{p} = 1 \times 10^{-9}$ m (plain curves), $\Delta\lambda_\mathrm{p} = 7 \times 10^{-10}$ m (curves with $*$), $\Delta\lambda_\mathrm{p} = 5 \times 10^{-10}$ m (curves with $\triangle$), and $\Delta\lambda_\mathrm{p} = 3 \times 10^{-10}$ m (curves with $\diamond$); log denotes decimal logarithm; $w_\mathrm{p} = 1 \times 10^{-3}$ m.

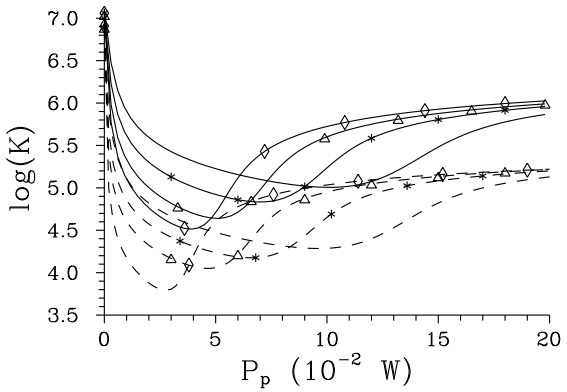

FIG. 2: Numbers K of twin-beam modes for 4-mm (solid curves) and 8-mm (dashed curves) long crystals as they depend on pump power P_p for $\Delta\lambda_\mathrm{p} = 1\times10^{-9}$ m (plain curves), $\Delta\lambda_\mathrm{p} = 7\times10^{-10}$ m (curves with $*$), $\Delta\lambda_\mathrm{p} = 5\times10^{-10}$ m (curves with $\triangle$), and $\Delta\lambda_\mathrm{p} = 3\times10^{-10}$ m (curves with $\diamond$); log denotes decimal logarithm; $w_\mathrm{p} = 1 \times 10^{-3}$ m.

8-mm long crystal and thus a greater number of down-converted modes faces pump depletion. For comparison, only around 1 % of the pump-pulse energy is transferred to the down-converted fields of the 8-mm long crystal for $P_{\rm p} \approx 0.2$ W, whereas around 8 % of the pump-pulse energy occurs in the down-converted fields of the 4-mm long crystal.

The curves in Fig. 2 show that the number K of modes considered as a function of power $P_{\rm p}$ reaches minimum for a certain threshold value $P_{\rm p,th}$. The comparison of curves in Figs. 1 and 2 reveals that this threshold power $P_{\rm p}$ determines a boundary between the areas with exponential and linear growths of the twin-beam intensity. Moreover, as discussed in the next subsection it also characterizes the power at which maximal coherence of the twin beam is reached. It is worth noting that the number K of modes of the 8-mm long crystal is smaller than that of the 4-mm long crystal assuming the pump-beam parameters fixed. This originates in more strict phase-matching conditions of the longer crystal.

B. Spectral coherence

The number of modes present in a twin beam determines its coherence. As follows from the comparison of curves in Figs. 3(a) and 4 giving the widths $\Delta C_{\rm s,\omega}$ of spectral intensity cross-correlation function and number K_ω^Δ of spectral modes for different pump spectral widths, the greater the number K_ω^Δ of spectral modes, the narrower the width $\Delta C_{\rm s,\omega}$ of spectral intensity cross-correlation function. This behavior stems from the properties of the spectral Schmidt modes. A q-th mode has $q-1$ minima in its intensity profile. Also, the larger the mode index q, the more complex the phase profile of the mode. The increasing power $P_{\rm p}$ prefers the modes with small numbers q (and great values of the Schmidt coefficients λ_{mlq}) which naturally leads to the broadening of the intensity spectral cross-correlation function. When the threshold value $P_{\rm r,th}$ of the power is reached, the number K_ω^Δ of spectral modes begins to increase, modes with greater values of index q become more important and, as a consequence, the twin-beam spectral coherence decreases. The pump spectral width $\Delta\lambda_{\rm p}$ and crystal length L are two critical parameters determining the spectral coherence of twin beam. Decrease of the pump spectral width $\Delta\lambda_{\rm p}$ (until certain width is reached [13, 32]) results in the decrease of the number K_ω^Δ of spectral modes, which leads to the growth of spectral coherence and, hand in hand, to lower values of the threshold power $P_{\rm p,th}$.

The spectra of down-converted fields as well as their intensity auto- and cross-correlation functions for the 8-mm long crystal are narrower than those of the 4-mm long crystal due to the more strict phase-matching conditions along the z axis [compare the solid and dashed curves in Fig. 3(a)]. The number K_ω^Δ of spectral modes in the longer crystal is greater compared to the shorter

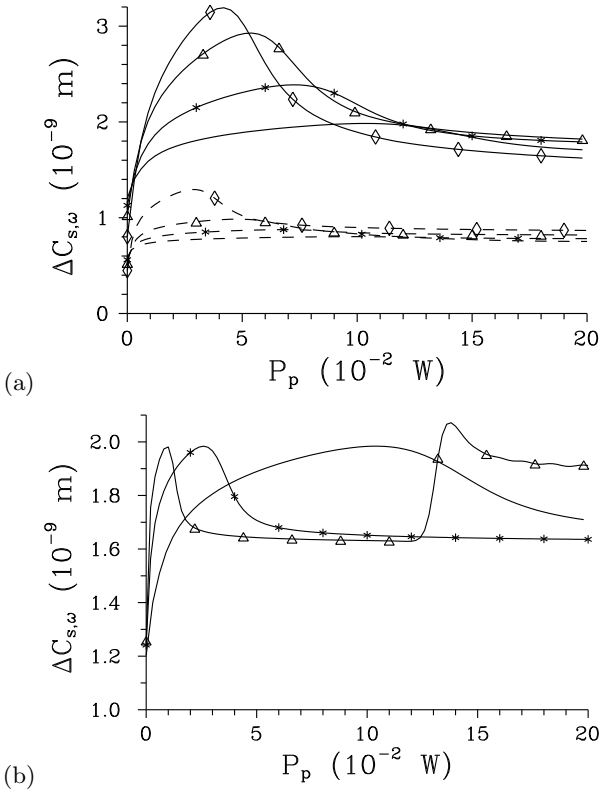

FIG. 3: Widths $\Delta C_{\rm s,\omega}$ of spectral intensity cross-correlation functions (FWHM, full width at half maximum) as they depend on pump power $P_{\rm p}$ for 4-mm (solid curves) and 8-mm (dashed curves) long crystals for (a) $\Delta\lambda_{\rm p} = 1\times10^{-9}$ m (plain curves), $\Delta\lambda_{\rm p} = 7\times10^{-10}$ m (curves with $*$), $\Delta\lambda_{\rm p} = 5\times10^{-10}$ m (curves with $\triangle$), and $\Delta\lambda_{\rm p} = 3\times10^{-10}$ m (curves with $\diamond$); $w_{\rm p} = 1\times10^{-3}$ m and (b) $w_{\rm p} = 1\times10^{-3}$ m (plain curve), $w_{\rm p} = 5\times10^{-4}$ m (curve with $*$) and $w_{\rm p} = 3\times10^{-4}$ m (curve with $\triangle$); $\Delta\lambda_{\rm p} = 1\times10^{-9}$ m.

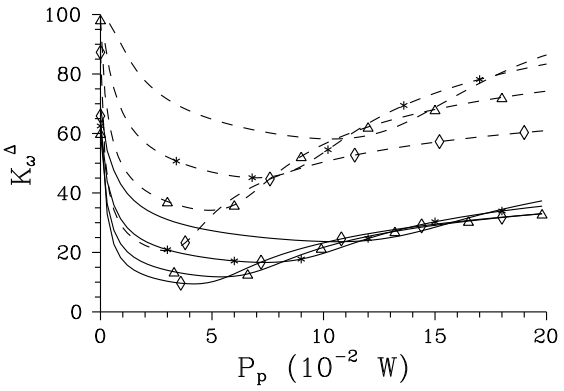

FIG. 4: Numbers K_ω^Δ of spectral modes given by the Fedorov ratio versus the pump power $P_{\rm p}$ for 4-mm (solid curves) and 8-mm (dashed curves) long crystals for $\Delta\lambda_{\rm p} = 1\times10^{-9}$ m (plain curves), $\Delta\lambda_{\rm p} = 7\times10^{-10}$ m (curves with $*$), $\Delta\lambda_{\rm p} = 5\times10^{-10}$ m (curves with $\triangle$), and $\Delta\lambda_{\rm p} = 3\times10^{-10}$ m (curves with $\diamond$); $w_{\rm p} = 1\times10^{-3}$ m.

crystal under the same conditions (compare the solid and dashed curves in Fig. 4). However, the overall numbers of spatio-spectral modes of the longer crystal are smaller (see Fig. 2) and so the threshold powers $P_{\mathrm{p,th}}$ determined for the longer crystal are smaller. Also, the longer interaction length of the 8-mm long crystal and thus the more intense energy transfer in this crystal contribute to the smaller threshold powers $P_{\mathrm{p,th}}$.

The pump-beam radius w_{p} influences the spectral coherence only indirectly, through the number of modes. The number of transverse modes decreases with the decreasing pump-beam radius w_{p} (for details, see [20]). Individual modes' triplets then attain greater pump-field energies and the effect of pump depletion occurs for smaller powers P_{p}. As a consequence, the maxima in the spectral coherence are reached for smaller threshold powers $P_{\mathrm{p,th}}$, as documented in Fig. 3(b). The maximal attainable value of the width $\Delta C_{\mathrm{s},\omega}$ of spectral intensity cross-correlation function is practically not affected by the pump-beam radius w_{p}.

For the analyzed range of pump powers P_{p}, the intensity auto- $A_{\mathrm{s},\omega}$ and cross-correlation $C_{\mathrm{s},\omega}$ functions practically coincide [13]. Spectra of the down-converted beams considered as functions of the power P_{p} behave in the opposed way than the correlation functions, i.e. they are becoming narrower with the increasing power P_{p} until the threshold power $P_{\mathrm{p,th}}$ is reached. For greater powers P_{p} they broaden. This behavior originates in the fact that the intensity spectral mode profiles $|f_{\mathrm{s},q}(\omega)|^2$ broaden with the increasing index q. As the modes with small numbers q dominate in the area around the threshold power $P_{\mathrm{p,th}}$, the spectra are narrower there.

Spectral coherence of the twin beam is also affected by the pump-pulse chirp parameter a_{p}. In general, a nonzero chirp parameter a_{p} introduces additional phase modulation to the two-photon spectral amplitude in the direction perpendicular to the direction $\omega_{\mathrm{s}} + \omega_{\mathrm{i}} = \mathrm{const}$. This influences the Schmidt decomposition. If the pump-field spectrum is sufficiently narrow (and enforces more strict conditions for the nonlinear interaction compared to the phase-matching condition along the z axis), the more complex phase modulation caused by the chirp results in greater numbers K_{ω}^{Δ} of spectral modes. That is why the twin-beam spectral coherence decreases with the increasing chirp parameter a_{p} and also the threshold power $P_{\mathrm{p,th}}$ increases (see the solid curves in Fig. 5 obtained for the pump-field spectrum 0.3 nm wide). On the other hand, if the pump-field spectrum is broader such that the phase-matching condition along the z axis causes a larger phase modulation, interference of this modulation with that coming from the pump-field chirp occurs. This may result in the increase of spectral coherence, as documented in Fig. 5 for the pump-field spectrum 0.7 nm wide.

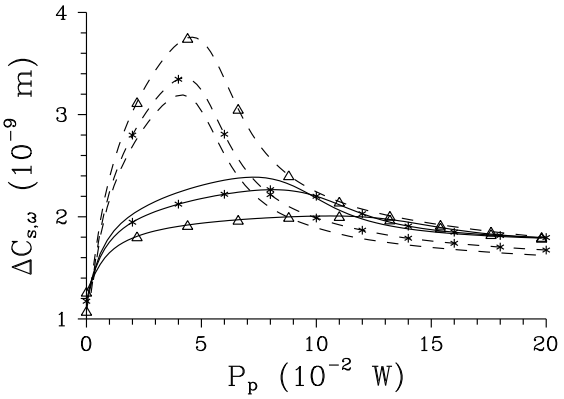

FIG. 5: Widths $\Delta C_{\mathrm{s},\omega}$ of intensity cross-correlation functions (FWHM) as they depend on pump power P_{p} for $\Delta\lambda_{\mathrm{p}} = 3 \times 10^{-10}$ m (solid curves) and $\Delta\lambda_{\mathrm{p}} = 7\times10^{-10}$ m (dashed curves) assuming $a_{\mathrm{p}} = 0$ (plain curves), $a_{\mathrm{p}} = 0.5$ (curves with $*$) and $a_{\mathrm{p}} = 1$ (curves with $\triangle$); $w_{\mathrm{p}} = 1 \times 10^{-3}$ m, $L = 4 \times 10^{-3}$ m.

C. Spatial coherence

Spatial coherence of the twin beam defined in the wavevector transverse plane (far field) behaves qualitatively in the same way as the spectral coherence provided that we consider the pump-beam radius w_{p} instead of the pump-field spectral width $\Delta\lambda_{\mathrm{p}}$. Coherence in the radial as well as azimuthal directions of the transverse plane increases with the decreasing pump-beam radius w_{p} [see Fig. 6(a) for the radial direction and Fig. 6(b) for the azimuthal direction]. This behavior stems from the decrease of the number of Schmidt modes in the transverse plane observed for the decreasing pump-beam radius w_{p} (for details, see [13]). Similarly as in the spectral domain, this is accompanied by decreasing values of the threshold power $P_{\mathrm{p,th}}$. Contrary to the maximal widths $\Delta C_{\mathrm{s},k}$ and $\Delta C_{\mathrm{s},\varphi}$ of the radial and azimuthal intensity cross-correlation functions, respectively, the threshold powers $P_{\mathrm{p,th}}$ depend also on the pump-field spectral width $\Delta\lambda_{\mathrm{p}}$. As the number K of modes decreases with the decreasing spectral width $\Delta\lambda_{\mathrm{p}}$, the threshold power $P_{\mathrm{p,th}}$ also decreases.

It is worth noting that, in Fig. 6, the azimuthal widths $\Delta C_{\mathrm{s},\varphi}$ are approx. 7-times wider than the radial widths $\Delta C_{\mathrm{s},k}$. This is caused by the strong influence of the phase-matching condition along the z axis when determining the radial correlation functions. Despite this, the influence of pump power P_{p} to the coherence is quite similar in both cases. We note that the intensity auto- and cross-correlation functions nearly coincide in both radial and azimuthal directions for the analyzed range of powers P_{p}.

The number of modes in the transverse plane is typically by several orders in magnitude larger than the number K_{ω}^{Δ} of spectral modes. On the other hand, the number of modes in the radial direction is usually of the same order as the number of spectral modes. Moreover, their

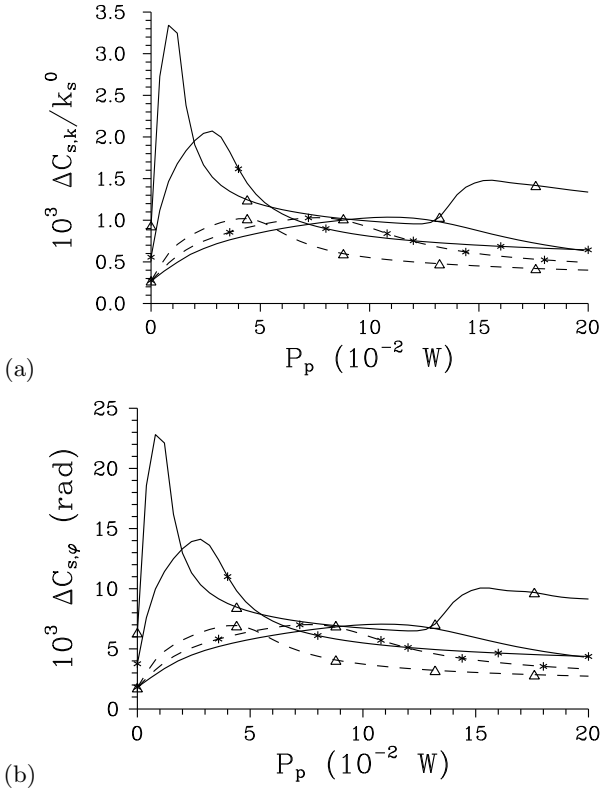

FIG. 6: (a) [(b)] Widths $\Delta C_{s,k}$ [$\Delta C_{s,\varphi}$] of radial [azimuthal] transverse intensity cross-correlation functions (FWHM) as they depend on pump power P_p for $\Delta\lambda_p = 1\times10^{-9}$ m, $w_p = 1\times10^{-3}$ m (plain solid curve), $w_p = 5\times10^{-4}$ m (solid curve with $*$), $w_p = 3\times10^{-4}$ m (solid curve with $\triangle$) and $w_p = 1\times10^{-3}$ m, $\Delta\lambda_p = 7\times10^{-10}$ m (dashed curve with $*$), $\Delta\lambda_p = 3\times10^{-10}$ m (dashed curve with $\triangle$); $L = 4\times10^{-3}$ m.

profiles behave in the similar way as the profiles of the spectral modes. That is why, we observe narrowing of the emission ring with the increasing power P_p until the threshold value $P_{p,th}$ is reached. The ring then widens with the increasing power P_p. Comparing the 4-mm and 8-mm long crystals, the number of radial modes is larger in the shorter crystal whereas the number of azimuthal modes is similar in both crystals.

We note that the Fourier transform of mode profiles in the transverse wave-vector plane gives the Schmidt mode profiles in the crystal output plane. These modes, however, have a specific structure analyzed in [13] that assures practical independence of the intensity correlation functions on the pump power P_p.

D. Temporal coherence

Temporal intensity auto- and cross-correlation functions mutually differ. The intensity auto-correlation functions $A_{s,t}$ are in general narrower than their cross-correlation counterparts $C_{s,t}$ (see Fig. 7). Their behavior with respect to the change of pump power P_p depends

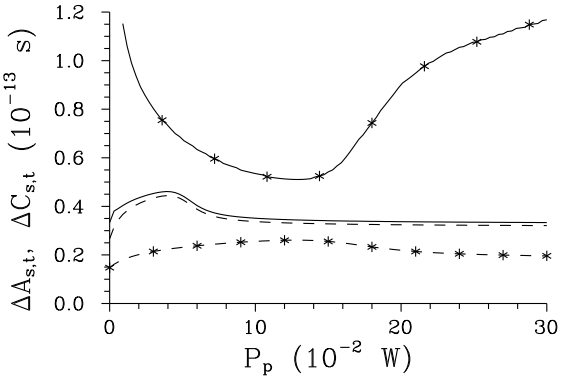

FIG. 7: Widths $\Delta C_{s,t}$ (solid curves) and $\Delta A_{s,t}$ (dashed curves) of temporal intensity auto- and cross-correlation functions (FWHM) as they depend on pump power P_p for $\Delta\lambda_p = 3\times10^{-10}$ m (plain curves) and $\Delta\lambda_p = 1.2\times10^{-9}$ m (curves with $*$); $w_p = 1\times10^{-3}$ m, $L = 4\times10^{-3}$ m.

on the pump-field spectral width $\Delta\lambda_p$. Provided that the pump-field spectral width $\Delta\lambda_p$ is sufficiently small, the auto- and cross-correlation functions behave in the same way as their spectral counterparts. Both of them exhibit their maxima at the threshold pump power $P_{p,th}$ determined in the spectral domain [compare the curves in Figs. 7 and 3(a) for $\Delta\lambda_p = 3\times10^{-10}$ m]. This behavior can be explained in the same way as in the spectrum because the profiles of temporal modes are similar to those of the spectral modes. We note that the Schmidt-mode structure and the varying mean photon numbers of the modes suppress the natural characteristic of the Fourier transform that assigns longer pulses to narrower spectra.

However, when the pump-field spectral width $\Delta\lambda_p$ is wider so that the nonlinear phase mismatch introduces greater phase modulations in the two-photon spectral amplitude, we observe decrease in the width $\Delta C_{s,t}$ of intensity cross-correlation function for the pump powers around $P_{p,th}$ (see the solid curve drawn for $\Delta\lambda_p = 1.2\times10^{-9}$ m in Fig. 7). In this area, the twin beam is composed of a reduced number of spectral modes that have the greatest Schmidt coefficients λ and exhibit only mild phase modulation. The strong phase spectral modulation described in a weak twin beam by the modes with smaller Schmidt coefficients are suppressed thus allowing shortening of the temporal cross-correlations. The intensity auto-correlation function $A_{s,t}$ is not sensitive to the phase modulation and so it evolves with the pump power P_p in the same manner as its spectral counterpart. Also, the signal-field pulse duration shortens with the increasing power P_p up to its threshold value $P_{p,th}$, where it begins to lengthen.

IV. MULTIPLE COHERENCE MAXIMA

The origin of coherence maxima discussed above and observed simultaneously in the spectrum (see Fig. 8) and

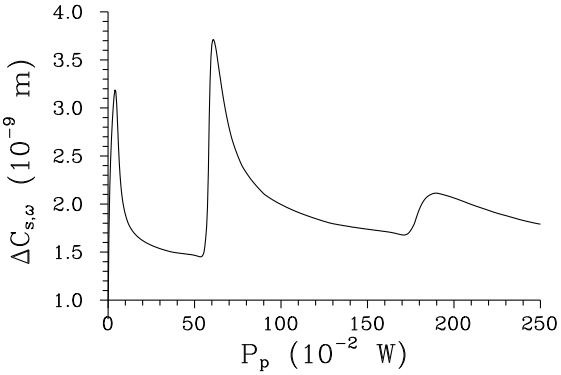

FIG. 8: Width $\Delta C_{\mathrm{s},\omega}$ of spectral intensity cross-correlation functions (FWHM) as it depends on pump power P_p; $\Delta\lambda_\mathrm{p} = 3\times10^{-10}$ m, $w_\mathrm{p} = 1\times10^{-3}$ m, $L = 4\times10^{-3}$ m.

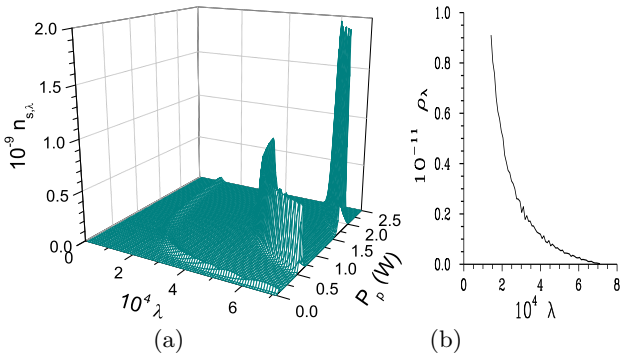

FIG. 9: (Color online) (a) Mean number $n_{\mathrm{s},\lambda}$ of signal photons in modes with the Schmidt coefficients λ as they depend on pump power P_p and (b) density ϱ_λ of modes revealed by the Schmidt decomposition; $n_\lambda = \langle \hat{a}^\dagger_{\mathrm{s},mlq}\hat{a}_{\mathrm{s},mlq}\rangle$ for mlq such that $\lambda_{ml}\lambda_q = \lambda$; parameters are given in the caption to Fig. 8.

radial and azimuthal directions in the wave-vector transverse plane has been explained by the reduction of the number of spatio-spectral twin-beam modes. This reduction is a consequence of different evolution of the mean photon numbers in the down-converted modes belonging to different modes' triplets. The modes with the greatest Schmidt coefficients λ take energy from the corresponding pump modes faster and so they grow more rapidly. That is why, they completely deplete their pump modes for smaller powers P_p (keeping the crystal length fixed) and reach their maximal mean photon numbers $n_{\mathrm{s},\lambda}$ [see Fig. 9(a)]. For larger powers P_p, the down-converted modes reach their maximal photon numbers inside the crystal and they return certain part of their energy back to their pump modes before leaving the crystal. For certain pump power depending on the triplet, the down-converted modes of the appropriate triplet leave the crystal in the vacuum state. Above this power, the triplet's evolution repeats from the beginning. As a consequence, the modes with the greatest Schmidt coefficients λ again reach their maximal mean photon numbers $n_{\mathrm{s},\lambda}$ for a sufficiently high power $P_{\mathrm{p,th1}}$. These maximal photon numbers are now considerably greater than those reached for $P_{\mathrm{p,th}}$ as the incident power P_p is greater and the mode structure is assumed independent on the pump power. Owing to the same reason as discussed for the powers around $P_{\mathrm{p,th}}$, there again occur local maxima in the spectral and spatial intensity correlation functions. As the incident pump powers belonging to individual modes' triplets are greater compared to those found around the power $P_{\mathrm{p,th}}$, the effect of modes' number reduction is even stronger and so even wider intensity correlation functions are observed. However, the coherence properties in this case are influenced also by another group of modes with smaller Schmidt coefficients [see Fig. 9(a)]. These modes have much lower mean photon numbers compared to the modes with the greatest Schmidt coefficients on one hand, on the other hand their number is much larger [see the density ϱ_λ of modes plotted in Fig. 9(b)]. They form a narrower peak in the intensity cross-correlation function $C_{\mathrm{s},\omega}$, on the top of a broader peak created by the modes with the greatest Schmidt coefficients λ (see Fig. 10). For the range of powers P_p investigated in Fig. 8, we even observe the third threshold power $P_{\mathrm{p,th2}}$. As three different groups of modes coexist in the twin beam for the powers around $P_{\mathrm{p,th2}}$, the coherence peak is less pronounced. Also, the profile of intensity cross-correlation function $C_{\mathrm{s},\omega}$ is more complex. This behavior is illustrated in Fig. 10 where the profile of cross-correlation function $C_{\mathrm{s},\omega}$ is drawn for the pump powers $P_\mathrm{p} \approx 0$ W, $P_{\mathrm{p,th}}$, $P_{\mathrm{p,th1}}$, and $P_{\mathrm{p,th2}}$.

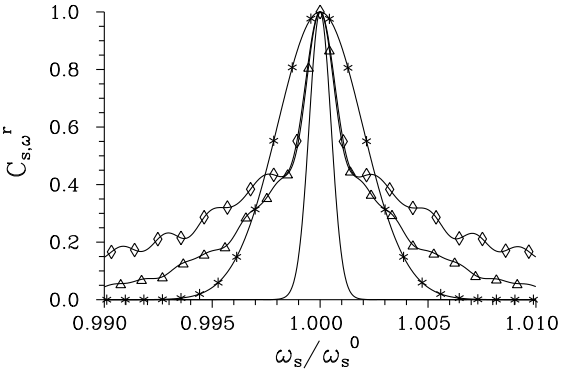

FIG. 10: Spectral intensity cross-correlation functions $C^\mathrm{r}_{\mathrm{s},\omega}(\omega_\mathrm{s}) \equiv C_{\mathrm{s},\omega}(\omega_\mathrm{s},\omega_\mathrm{i}^0)/C_{\mathrm{s},\omega}(\omega_\mathrm{s}^0,\omega_\mathrm{i}^0)$ are plotted for $P_\mathrm{p} = 1\times10^{-7}$ W (plain curve), $P_\mathrm{p} = 4\times10^{-2}$ W (curve with $*$); $P_\mathrm{p} = 6.1\times10^{-1}$ W (curve with $\triangle$), and $P_\mathrm{p} = 1.3$ W (curve with $\diamond$); parameters are given in the caption to Fig. 8.

V. MODEL WITH THE EXTENDED CRYSTAL LENGTH

In the crystals like BBO in the considered type-I interaction configuration there occurs walk-off of the interacting fields due to anisotropy of the pump beam [32]. Owing to the walk-off, the modes' triplets interacting at the beginning of the crystal gradually loose their mutual

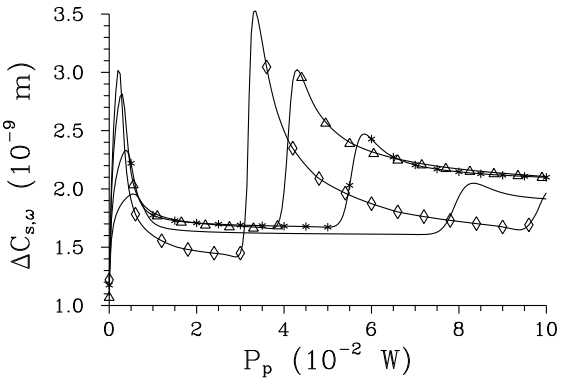

FIG. 11: Widths $\Delta C_{\mathrm{s},\omega}$ of spectral intensity cross-correlation functions (FWHM) as they depend on pump power P_p for $\Delta\lambda_\mathrm{p} = 1\times10^{-9}$ m (plain curve), $\Delta\lambda_\mathrm{p} = 7\times10^{-10}$ m (curves with $*$), $\Delta\lambda_\mathrm{p} = 5\times10^{-10}$ m (curves with $\triangle$), and $\Delta\lambda_\mathrm{p} = 3\times10^{-10}$ m (curves with $\diamond$); $w_\mathrm{p} = 5\times10^{-4}$ m, $L = 4\times10^{-3}$ m, $L_\mathrm{ext} = 8\times10^{-3}$ m.

overlap in the transverse plane which effectively weakens the nonlinear interaction. On the other hand, new modes' triplets can be seeded as the pump beam propagates along the crystal. This poses the question about an effective interaction length for individual modes' triplets and also about an appropriate crystal length that determines the Schmidt-mode profiles. We note that the shorter the crystal, the wider the spectral and radial spatial modes. This affects coherence of the twin beam. The developed model is not able to incorporate the influence of crystal anisotropy directly. On the other hand, we may consider two different crystal lengths in the model. The first length L determines the extension of mode profiles whereas the second length L_ext characterizes an effective length of the nonlinear interaction.

To reveal the main features of the twin beams in such a model, we consider a crystal 8-mm long and twin-beam modes appropriate for a 4-mm long crystal. Widths $\Delta C_{\mathrm{s},\omega}$ of spectral intensity cross-correlation functions depending on the pump power P_p are plotted in Fig. 11 for several pump-field spectral widths $\Delta\lambda_\mathrm{p}$. The comparison of widths $\Delta C_{\mathrm{s},\omega}$ drawn in Fig. 11 with those plotted in Fig. 3(a) for the crystal 4-mm long reveals that the maximal spectral widths $\Delta C_{\mathrm{s},\omega}$ are approximately the same for both cases. However, the threshold pump powers $P_{\mathrm{p,th}}$ are more than 4-times lower for the 8-mm long crystal. This arises from the fact that the interaction strength scales as $L\sqrt{P_\mathrm{p}}$. In other words, a crystal two times longer needs only one quarter of the incident power to provide the same interaction. The vacuum contributions to the evolution of modes' triplets even move the threshold powers $P_{\mathrm{p,th}}$ to slightly lower values. For this reason, we observe the second threshold powers $P_{\mathrm{p,th1}}$ in Fig. 11 for the pump powers P_p considerably lower than in the case of the 4-mm long crystal.

VI. CONCLUSIONS

Using the spatio-spectral Schmidt dual signal and idler modes and the corresponding pump modes, we have developed the model of intense parametric down-conversion applicable in the regime with pump depletion. Contrary to the usual parametric approximation, the model assumes a classical pump beam that undergoes depletion during its propagation (*the generalized parametric approximation*). Due to the pump depletion, the initial increase of spectral, temporal and transverse wavevector coherence on the pump-power axis is replaced by a decrease. This occurs as a consequence of the backflow of energy from the down-converted modes into the pump modes observed in the most strongly interacting modes' triplets (with the greatest Schmidt coefficients). The change of twin-beam coherence reflects the relative change of mean photon numbers in individual twin-beam modes. The better the coherence the smaller the number of well-populated modes and vice versa. The threshold pump power at which the best coherence is reached has been analyzed as it depends on the pump spectral width and spatial radius. The relationship between the coherence and the twin-beam mode structure predicts the existence of additional threshold pump powers at which the local coherence functions reach their maxima. The curves obtained for the 4-mm and 8-mm long BBO crystals in the typical experimental configuration have provided a deeper insight into the twin-beam properties useful, e.g., in interpreting the experimental results.

Acknowledgments

The author thanks M. Bondani, J. Peřina, O. Haderka, A. Allevi and O. Jedrkiewicz for stimulating discussions. He gratefully acknowledges the support by project 15-08971S of the Grant Agency of the Czech Republic and project LO1305 of the Ministry of Education, Youth and Sports of the Czech Republic.

[1] O. Jedrkiewicz, Y. K. Jiang, E. Brambilla, A. Gatti, M. Bache, L. A. Lugiato, and P. Di Trapani. Detection of sub-shot-noise spatial correlation in high-gain parametric down-conversion. *Phys. Rev. Lett.*, 93:243601, 2004.

[2] M. Bondani, A. Allevi, G. Zambra, M. G. A. Paris, and A. Andreoni. Sub-shot-noise photon-number correlation in a mesoscopic twin beam of light. *Phys. Rev. A*, 76:013833, 2007.

[3] J.-L. Blanchet, F. Devaux, L. Furfaro, and E. Lantz. Measurement of sub-shot-noise correlations of spatial fluctuations in the photon-counting regime. *Phys. Rev. Lett.*, 101:233604, 2008.

[4] G. Brida, L. Caspani, A. Gatti, M. Genovese, A. Meda, and I. R. Berchera. Measurement of sub-shot-noise spatial correlations without backround subtraction. *Phys. Rev. Lett.*, 102:213602, 2009.

[5] R. Machulka, O. Haderka, J. Peřina Jr, M. Lamperti, A. Allevi, and M. Bondani. Spatial properties of twin-beam correlations at low- to high-intensity transition. *Opt. Express*, 22:13374—13379, 2014.

[6] A. Allevi and M. Bondani. Statistics of twin-beam states by photon-number resolving detectors up to pump depletion. *J. Opt. Soc. Am. B*, 31:B14—B19, 2014.

[7] A. Christ, K. Laiho, A. Eckstein, K. N. Cassemiro, and C. Silberhorn. Probing multimode squeezing with correlation functions. *New J. Phys.*, 13:033027, 2011.

[8] K. Y. Spasibko, T. S. Iskhakov, and M. V. Chekhova. Spectral properties of high-gain parametric down-conversion. *Opt. Express*, 20:7507—7515, 2012.

[9] A. Christ, B. Brecht, W. Mauerer, and C. Silberhorn. Theory of quantum frequency conversion and type-II parametric down-conversion in the high-gain regime. *New J. Phys.*, 15:053038, 2013.

[10] A. M. Pérez, T. S. Iskhakov, P. Sharapova, S. Lemieux, O. V. Tikhonova, M. V. Chekhova, and G. Leuchs. Bright squeezed-vacuum source with 1.1 spatial mode. *Opt. Lett.*, 39:2403—2406, 2014.

[11] B. Brecht, A. Eckstein, R. Ricken, V. Quiring, H. Suche, L. Sansoni, and C. Silberhorn. Demonstration of coherent time-frequency Schmidt mode selection using dispersion-engineered frequency conversion. *Phys. Rev. A*, 90:030302(R), 2014.

[12] P. Sharapova, A. M. Pérez, O. V. Tikhonova, and M. V. Chekhova. Schmidt modes in the angular spectrum of bright squeezed vacuum. *Phys. Rev. A*, 91:043816, 2015.

[13] J. Peřina Jr. Coherence and mode decomposition of intense twin beams. *Phys. Rev. A*, 92:013833, 2015.

[14] A. Allevi, O. Jedrkiewicz, E. Brambilla, A. Gatti, J. Peřina Jr., O. Haderka, and M. Bondani. Coherence properties of high-gain twin beams. *Phys. Rev. A*, 90:063812, 2014.

[15] A. Allevi, O. Jedrkiewicz, O. Haderka, J. Peřina Jr., and M. Bondani. Evolution of spatio-spectral coherence properties of twin beam states in the high gain regime. In K. Banaszek and C. Silberhorn, editors, *Proc. of SPIE 9505*, page 95050S, Bellingham, 2015. SPIE.

[16] A. Allevi, M. Lamperti, R. Machulka, O. Jedrkiewicz, E. Brambilla, A. Gatti, J. Peřina Jr., O. Haderka, and M. Bondani. Effects of pump depletion on spatial and spectral properties of parametric down-conversion. In K. Banaszek and C. Silberhorn, editors, *Proc. of SPIE 9505*, page 950508, Bellingham, 2015. SPIE.

[17] C. K. Law, I. A. Walmsley, and J. H. Eberly. Continuous frequency entanglement: Effective finite Hilbert space and entropy control. *Phys. Rev. Lett.*, 84:5304—5307, 2000.

[18] C. K. Law and J. H. Eberly. Analysis and interpretation of high transverse entanglement in optical parametric down-conversion. *Phys. Rev. Lett.*, 92:127903, 2004.

[19] M. V. Fedorov and M. I. Miklin. Schmidt modes and entanglement. *Contemporary Phys.*, 55:94—109, 2014.

[20] J. Peřina Jr. Coherence and mode decomposition of weak twin beams. *Phys. Scr.*, 90:074058, 2015.

[21] E. Brambilla, A. Gatti, M. Bache, and L. A. Lugiato. Simultaneous near-field and far-field spatial quantum correlations in the high-gain regime of parametric down-conversion. *Phys. Rev. A*, 69:023802, 2004.

[22] A. Gatti, R. Zambrini, M. San Miguel, and L. A. Lugiato. Multiphoton multimode polarization entanglement in parametric down-conversion. *Phys. Rev. A*, 68:053807, 2003.

[23] E. Brambilla, L. Caspani, L. A. Lugiato, and A. Gatti. Spatiotemporal structure of biphoton entanglement in type-II parametric down-conversion. *Phys. Rev. A*, 82:013835, 2010.

[24] L. Caspani, E. Brambilla, and A. Gatti. Tailoring the spatiotemporal structure of biphoton entanglement in type-I parametric down-conversion. *Phys. Rev. A*, 81:033808, 2010.

[25] B. Dayan, Y. Bromberg, I. Afek, and Y. Silberberg. Spectral polarization and spectral phase control of time-energy entangled photons. *Phys. Rev. A*, 75:043804, 2007.

[26] R. W. Boyd. *Nonlinear Optics, 2nd edition*. Academic Press, New York, 2003.

[27] P. Kolchin, S. Du, Ch. Belthangady, G. Y. Yin, and S. E. Harris. Generation of narrow-bandwidth paired photons: Use of a single driving laser. *Phys. Rev. Lett.*, 97:113602, 2006.

[28] Q. Glorieux, R. Dubessy, S. Guibal, L. Guidoni, J.-P. Likforman, T. Coudreau, and E. Arimondo. Double-λ microscopic model for entangled light generation by four-wave mixing. *Phys. Rev. A*, 82:033819, 2010.

[29] V. Boyer, A. M. Marino, R. C. Pooser, and P. D. Lett. Entangled images from four-wave mixing. *Science*, 321:544—547, 2008.

[30] J. Peřina. *Quantum Statistics of Linear and Nonlinear Optical Phenomena*. Kluwer, Dordrecht, 1991.

[31] J. Peřina Jr. and J. Peřina. Quantum statistics of nonlinear optical couplers. In E. Wolf, editor, *Progress in Optics, Vol. 41*, pages 361—419. Elsevier, Amsterdam, 2000.

[32] M. V. Fedorov, M. A. Efremov, P. A. Volkov, E. V. Moreva, S. S. Straupe, and S. P. Kulik. Spontaneous parametric down-conversion: Anisotropical and anomalously strong narrowing of biphoton momentum correlation distributions. *Phys. Rev. A*, 77:032336, 2008.

[33] M. V. Fedorov, M. A. Efremov, P. A. Volkov, E. V. Moreva, S. S. Straupe, and S. P. Kulik. Anisotropical and high entanglement of biphoton states generated in spontaneous parametric down-conversion. *Phys. Rev. Lett.*, 99:063901, 2007.

[34] Y. M. Mikhailova, P. A. Volkov, and M. V. Fedorov. Biphoton wave packets in parametric down-conversion: Spectral and temporal structure and degree of entanglement. *Phys. Rev. A*, 78:062327, 2008.

[35] A. Gatti, T. Corti, E Brambilla, and D. B. Horoshko. Dimensionality of the spatiotemporal entanglement of parametric down-conversion photon pairs. *Phys. Rev. A*, 86:053803, 2012.

[36] D. B. Horoshko, G. Patera, A. Gatti, and M. I. Kolobov. X-entangled biphoton: Schmidt number for 2D model. *Eur. Phys. J. D*, 66:239, 2012.

[37] J. Peřina Jr. Pulsed-squeezed-light generation in a waveguide with second-subharmonic generation and periodic corrugation. *Phys. Rev. A*, 87:013833, 2013.

[38] M. Stobińska, F. Töppel, P. Sekatski, and M. V. Chekhova. Entanglement witnesses and measures for bright squeezed vacuum. *Phys. Rev. A*, 86:022323, 2012.

[39] M. V. Chekhova, G.Leuchs, and M. Zukowski. Bright

squeezed vacuum: Entanglement of macroscopic light beams. *Opt. Comm.*, 337:27—43, 2015.

[40] M. V. Fedorov, M. A. Efremov, A. E. Kazakov, K. W. Chan, C. K. Law, and J. H. Eberly. Spontaneous emission of a photon: Wave-packet structures and atom-photon entanglement. *Phys. Rev. A*, 72:032110, 2005.